

General structured light generation based on programmable linearly-polarized mode synthesizer

Wei Chen ^{1,†}, Fang Ren ^{2,†}, Yuyang Gao ^{1,2}, Xiaofeng Li ¹, Dawei Ge ¹, Zhangyuan Chen ¹,
Yongqi He ¹, and Juhao Li ^{1,3}

¹ State Key Laboratory of Advanced Optical Communication Systems and Networks, Peking University, Beijing 100871, China

² School of Computer and Communication Engineering, University of Science and Technology Beijing, Beijing 100083, China

³ Peng Cheng Laboratory, Shenzhen 518055, China

Abstract Fiber-based structured light including cylindrical vector beams (CVBs) and orbital angular momentum (OAM) has gained significant interest for its unique properties. In this work, we propose the concept of a programmable linearly-polarized (LP) -mode synthesizer for general structured light generation, in which an LP-mode pool supporting independent and selectable LP-mode output is first established, and then different CVB/OAM modes could be generated in a general way through polarization and phase control. We demonstrate a proof-of-concept LP-mode synthesizer based on a fiber ring laser characterized by a partial 5-LP mode weakly-coupled few-mode fiber (FMF) cavity and arbitrary LP-mode switch array. Various CVB/OAM beams including TE_{01} , TM_{01} , $OAM_{\pm 1}$, and $OAM_{\pm 2}$ modes are successfully generated. This approach provides new insights into mode manipulation

This peer-reviewed article has been accepted for publication but not yet copyedited or typeset, and so may be subject to change during the production process. The article is considered published and may be cited using its DOI.

This is an Open Access article, distributed under the terms of the Creative Commons Attribution licence (<https://creativecommons.org/licenses/by/4.0/>), which permits unrestricted re-use, distribution, and reproduction in any medium, provided the original work is properly cited.

10.1017/hpl.2025.10060

methods, potentially enhancing the performance of optical quantum communications, optical fiber sensing, and optical trapping applications.

Correspondence to: J. Li, State Key Laboratory of Advanced Optical Communication Systems and Networks, Peking University, Beijing 100871, China; F. Ren, School of Computer and Communication Engineering, University of Science and Technology Beijing, Beijing 100083, China.
 Emails: juhao_li@pku.edu.cn (J. Li); renfang@ustb.edu.cn (F. Ren)
 † These authors contributed equally

Key words: mode manipulation; structure light; cylindrical vector beam; orbital angular momentum; fiber laser

I. INTRODUCTION

Maneuvering different physical dimensions of photons including frequency, time, amplitude, phase, polarization, and spatial structure enables manifold light-related applications. In particular, fiber-based structured light beams such as CVBs and OAM modes have attracted increasing attention owing to their unique properties of spatial intensity, phase, and polarization distributions, which have promoted vigorous researches in optical and quantum communication systems^[1,2], optical sensing^[3,4], microscopy^[5,6], optical trapping^[7,8], and so on. For instance, additional phase change undergone by OAM beam helps to enhance sensing resolution for an interferometer application.^[4]

Various approaches have been proposed to generate these structured light in recent years. Discrete components such as spatial light modulators^[9,10], axial birefringent components^[11], specially designed laser cavities^[12-14], spiral phase plates^[15,16], and plasmonic metasurfaces^[17-20] have been utilized to reshape free-space Gaussian beams into CVBs/OAMs or to directly emit CVB/OAM beam. However, the bulk volume and complex optical alignment may hinder their practical applications. Meanwhile, approaches utilizing optical fiber-based components, lasing cavities, or optical circuits have also been widely investigated, such as long-period fiber gratings

[21-23], vortex grating [24], mode-selective couplers (MSCs) [25,26], and tapered fiber [27]. However, the lacking of a general method and extensibility to generate CVBs and OAMs may be their shared limitation.

Recent studies on the utilization of LP modes in weakly-coupled FMF transmission systems may provide a new way for the generation of fiber-based structured light. In these systems [28-31], the modal crosstalk for FMFs and matched mode multiplexers/demultiplexers (MMUXes/MDEMUXes) is significantly suppressed, so that light could independently propagate through multiple LP modes and the transmission capacity could be multiplied without inter-modal multiple-input multiple-output digital signal processing. Because the effective index difference ($|\Delta n_{eff}|$) is the dominant factor of distributed modal crosstalk between LP modes, step-index FMF with high core/cladding index difference and multiple-ring-core (MRC) FMF utilizing ring index perturbations to enlarge the minimum $|\Delta n_{eff}|$ among LP modes have been proposed for distributed modal crosstalk suppression [28,29]. Different kinds of MMUXes and MDEMUXes with low intrinsic channel crosstalk and coupling crosstalk have been adopted including photonic lanterns [31,32], multiple plane light converters [33,34], volume holograms [35], and cascaded MSCs [36,37]. Further, the independent LP manipulation capability could be utilized to generate fiber-based structured light by applying proper mode conversion.

In this paper, we propose the programmable LP-mode synthesizer as a general approach to generate fiber-based structured light. An LP-mode pool is first established to generate independent and selectable LP modes. Then, different CVB/OAM modes could be generated in accordance with the conversion relation with LP modes. We experimentally demonstrate the LP-mode synthesizer utilizing a 5-LP mode fiber ring laser with a partial weakly-coupled FMF cavity. The output LP mode could be controlled by an arbitrary LP-mode switch array, and a polarization

controller (PC) is employed for polarization and phase control. We last experimentally demonstrate the successful generation of various CVB/OAM beams including TE_{01} , TM_{01} , OAM_{+1} , OAM_{-1} , OAM_{+2} , and OAM_{-2} .

II. CONCEPT OF PROGRAMMABLE LP-MODE SYNTHESIZER

The conversion relations between LP modes and CVB/OAM modes are the theoretical basis for the proposed LP-mode synthesizer. As we know, the CVB modes and OAM modes are two eigenmode sets in optical fibers under the Cartesian coordinate system^[38] and the circular polarization coordinate system^[39], respectively. The polarization vector mode corresponds to the CVB mode whereas the phase vortex mode conveys the OAM mode. Mathematically, the LP modes are the solutions of scalar Helmholtz equations under the weakly-guiding approximation, and the superposition of near-degenerate CVB modes forms LP states. The relation of the LP modes and CVB modes could be described by^[40],

$$\begin{bmatrix} HE_{m+1,n}^e \\ HE_{m+1,n}^o \\ EH_{m-1,n}^e \\ EH_{m-1,n}^o \end{bmatrix} = F_{m,n}(r) \begin{bmatrix} 1 & 0 & 0 & -1 \\ 0 & 1 & 1 & 0 \\ 1 & 0 & 0 & 1 \\ 0 & -1 & 1 & 0 \end{bmatrix} \begin{bmatrix} \vec{e}_x \cos(m\varphi) \\ \vec{e}_y \cos(m\varphi) \\ \vec{e}_x \sin(m\varphi) \\ \vec{e}_y \sin(m\varphi) \end{bmatrix} = \begin{bmatrix} 1 & 0 & 0 & -1 \\ 0 & 1 & 1 & 0 \\ 1 & 0 & 0 & 1 \\ 0 & -1 & 1 & 0 \end{bmatrix} \begin{bmatrix} \vec{e}_x LP_{m,n}^e \\ \vec{e}_y LP_{m,n}^e \\ \vec{e}_x LP_{m,n}^o \\ \vec{e}_y LP_{m,n}^o \end{bmatrix} \quad (1)$$

where “e” and “o” represent the even and odd modes, $F_{m,n}(r)$ is the radial field distribution of the corresponding scalar mode (LP) solution, m is the azimuthal order of CVB modes, n is the radial order of CVB modes, r is the radial coordinate, and φ is the angular coordinate. In optical fiber waveguides, hybrid electric (HE) and hybrid magnetic (EH) modes are two classes of hybrid electromagnetic modes that exhibit both longitudinal electric and magnetic field component ($E_z \neq 0$ and $H_z \neq 0$), distinguishing them from purely transverse electric (TE) or transverse magnetic (TM) modes. Note that $EH_{m-1,n}^e$ is substituted by $TM_{0,n}$ and $EH_{m-1,n}^o$ is substituted by $TE_{0,n}$ when $m=1$.

Similarly, the OAM modes having a helical wave-front phase can be formed by the superposition of CVB modes ^[40]. So, the OAM modes in the fiber can be expressed as a linear superposition of the odd and even CVB modes with $\pm\pi/2$ phase difference. Generally, in the weakly-guiding fiber, the superposition of near-degenerate CVB modes forms LP states.

So, OAM modes can be expressed by,

$$\begin{bmatrix} \vec{\sigma}^+ OAM_{+m} \\ \vec{\sigma}^- OAM_{-m} \\ \vec{\sigma}^- OAM_{+m} \\ \vec{\sigma}^+ OAM_{-m} \end{bmatrix} = F_{m,n}(r) \begin{bmatrix} \vec{\sigma}^+ \exp(+jm\varphi) \\ \vec{\sigma}^- \exp(-jm\varphi) \\ \vec{\sigma}^- \exp(+jm\varphi) \\ \vec{\sigma}^+ \exp(-jm\varphi) \end{bmatrix} = \begin{bmatrix} 1 & j & j & -1 \\ 1 & -j & -j & -1 \\ 1 & -j & j & 1 \\ 1 & j & -j & 1 \end{bmatrix} \begin{bmatrix} \vec{e}_x LP_{m,n}^e \\ \vec{e}_y LP_{m,n}^e \\ \vec{e}_x LP_{m,n}^o \\ \vec{e}_y LP_{m,n}^o \end{bmatrix} \quad (2)$$

where $OAM_{\pm m}$ denote the field distributions of helical wave-front phase $\exp(\pm jm\varphi)$; the subscripts “ \pm ” of OAM separately correspond to the left-hand and right-hand helical wave-front phase. Especially, the combination of LP modes with a $\pm\pi/2$ phase difference in the weakly-guiding fiber can form linearly-polarized OAM modes ^[41],

$$\begin{bmatrix} \vec{e}_x OAM_{-m} \\ \vec{e}_y OAM_{-m} \\ \vec{e}_x OAM_{+m} \\ \vec{e}_y OAM_{+m} \end{bmatrix} = F_{m,n}(r) \begin{bmatrix} \vec{e}_x \exp(-jm\varphi) \\ \vec{e}_y \exp(-jm\varphi) \\ \vec{e}_x \exp(+jm\varphi) \\ \vec{e}_y \exp(+jm\varphi) \end{bmatrix} = \begin{bmatrix} 1 & 0 & -j & 0 \\ 0 & 1 & 0 & -j \\ 1 & 0 & j & 0 \\ 0 & 1 & 0 & j \end{bmatrix} \begin{bmatrix} \vec{e}_x LP_{m,n}^e \\ \vec{e}_y LP_{m,n}^e \\ \vec{e}_x LP_{m,n}^o \\ \vec{e}_y LP_{m,n}^o \end{bmatrix} \quad (3)$$

The schematic diagram of a programmable LP-mode synthesizer for CVB/OAM generation is illustrated in Figure 1, which interprets literally the mode conversion relations shown in Equations. (1)-(3). First, the LP-mode pool should be established to stock arbitrary LP modes

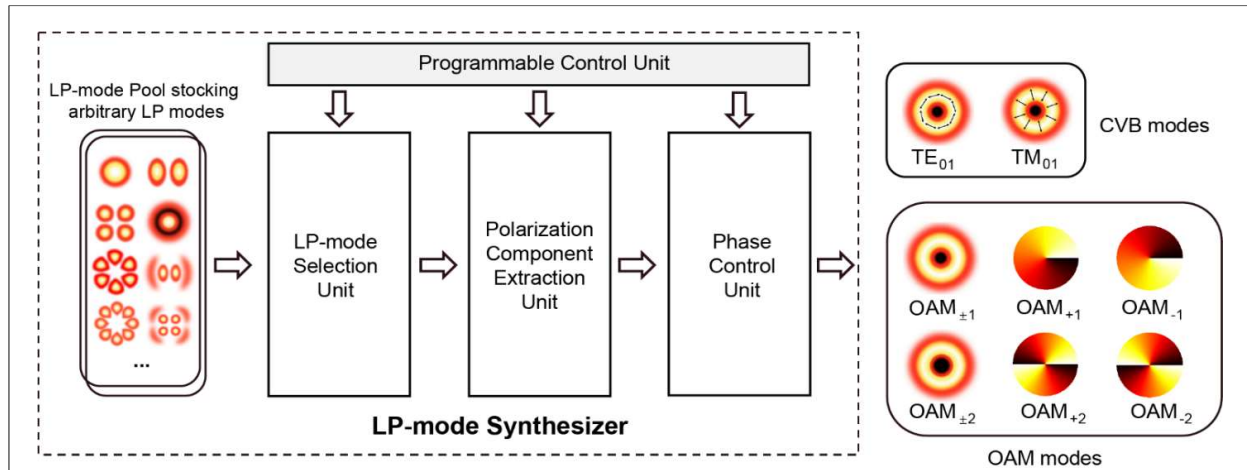
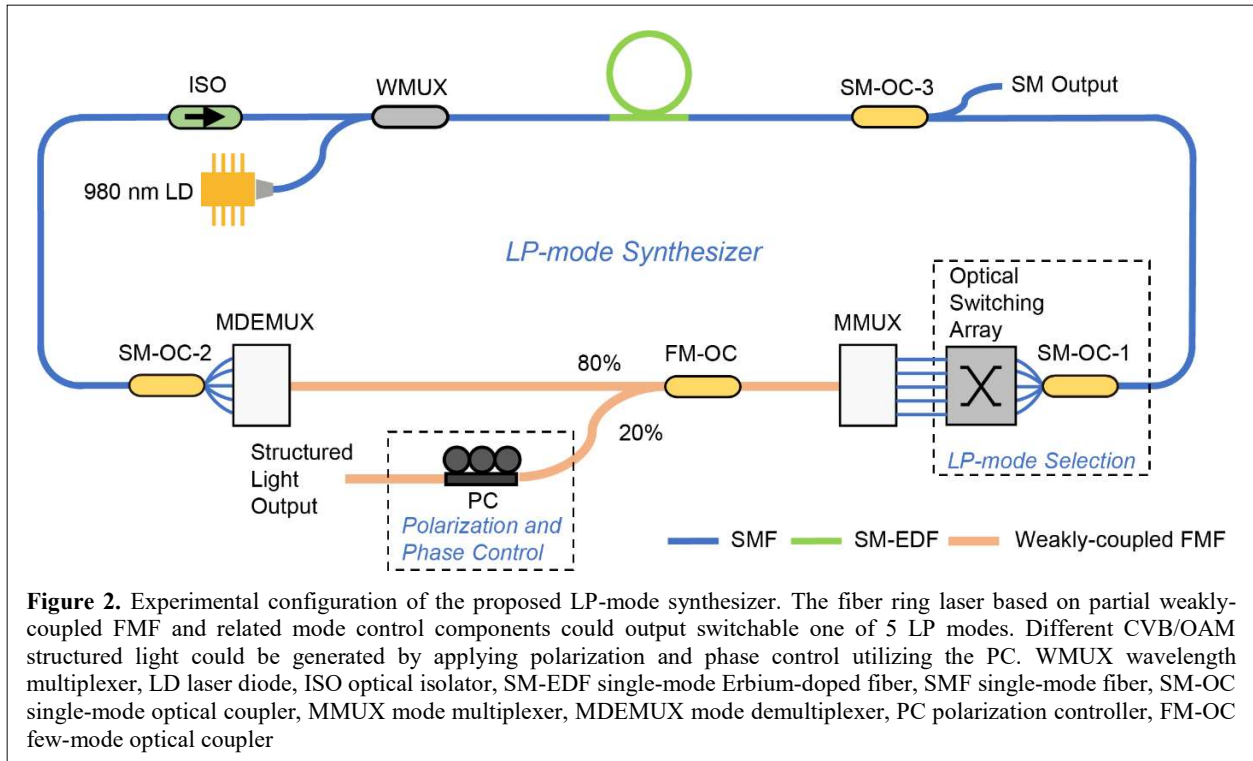


Figure 1. Schematic diagram of fiber-based CVB/OAM generation based on a programmable LP-mode synthesizer. The LP-mode pool based on weakly-coupled FMF circuits generates independent and selectable LP modes. The LP-mode selection unit selects a specific LP mode, the polarization component extraction unit separates different polarization components, while the phase control unit adjusts the phase difference. All the operations could be controlled by the programmable control unit according to the mode conversion relations.

and output them independently according to the need. The flexible selection of active LP mode in the LP-mode pool is obtained by the LP-mode selection unit. The polarization component extraction unit is used to detach the elements of the selected LP mode. After that, the phase differences among the elements are adjusted by the phase control unit. The programmable control unit is responsible for the configuration of the three units according to the conversion relations.

The physical implementations of the programmable LP-mode synthesizer may take flexible forms. The LP-mode pool accompanied with the LP-mode selection unit should output switchable LP mode in a general way, which could be realized by various simple and effective approaches based on commercial optical components such as LP-mode converters or MMUXes. There are also different kinds of approaches for polarization component extraction and phase delay utilizing fiber-based or free-space micro-structured optical elements such as polarization beam splitters and optical delay lines. It should be noted that the optical circuit in the programmable LP-mode



synthesizer should be built up based on weakly-coupled FMFs and matched low-modal-crosstalk mode control components to sustain the independence among the LP modes.

III. EXPERIMENTAL SETUP

Figure 2 shows the experimental configuration of a fiber ring laser to verify the feasibility of the LP-mode synthesizer, the cavity of which is composed of both single-mode fiber (SMF) and FMF sections. Different types of laser structures could serve as the LP-mode synthesizer. In the experiment, we adopt the fiber ring laser for multiple merits of low mode competition, high stability and all-fiber structure. In the FMF section, the weakly-coupled MRC FMF supports 6 LP modes, and the highest-order LP_{12} mode has large propagation loss and acts as a guarding mode, so independent light propagation can be achieved through 5 LP modes (LP_{01} , LP_{11} , LP_{21} , LP_{02} , LP_{31}) with very low modal crosstalk. The weakly-coupled FMF enables multiple LP modes to oscillate independently. Single-mode instead of few-mode gain fiber is adopted, which could

128 simplify the laser structure by eliminating the differential modal gain. The MMUX/MDEMUX
129 may take flexible forms. In the experiment, we adopt the cascaded MSCs. The MMUX/MDEMUX
130 consists of 5 cascaded MSCs, and it should be noted that each MSC could only perform mode
131 conversion between the fundamental mode in the SMF and one of a pair of degenerate LP modes
132 in the FMF. The integration of weakly-coupled FMF and matched MMUX/MDEMUX endows
133 the system with the functionality of LP modes selection and control. An 80:20 few-mode optical
134 coupler (FM-OC) is utilized as the output coupler of the laser, which is a free-space wave-plate
135 beam splitter and achieves better mode insensitivity than fused-type FM-OC ^[42]. A conventional
136 single-mode pump scheme is adopted in the SMF section, consisting of 980-nm laser diode (LD),
137 980/1550-nm wavelength multiplexer (WMUX) for pump/signal light combination, and a piece of
138 single-mode Erbium-doped fiber (SM-EDF) with the length of 5-m as the gain medium. The
139 optical isolator (ISO) enables unidirectional light propagation. The single-mode optical coupler-1
140 (SM-OC-1) is used to split the light into 5 branches. The higher-order modes are converted back
141 to LP₀₁ mode by the MDEMUX and then combined to the SMF through another SM-OC-2 for the
142 next round of signal circulation.

The MRC-FMF in the experimental setup is a customized weakly-coupled FMF fabricated by plasma chemical vapor deposition technique with the index profile shown in Figure 3(a) [29], and the n_{eff} distribution at the wavelength of 1550 nm is also plotted. The FMF is designed to support weakly-coupled MDM transmission for 6 LP modes [29], for which the overall performance is limited by the worst mode channel with the largest modal crosstalk. Since the n_{eff} of all the LP modes lies between the indexes of fiber core and cladding and the $|\Delta n_{eff}|$ is the dominant factor for modal crosstalk between LP modes, the best transmission performance could be achieved when the n_{eff} of all the LP modes is equally spaced. So, the weakly-coupled MRC-FMF is designed by applying two index perturbation regions to the core area of an initial step-index FMF to enlarge the minimum $|\Delta n_{eff}|$ among all LP modes. The minimum $|\Delta n_{eff}|$ of the weakly-coupled MRC-FMF is 1.49×10^{-3} lying between LP_{21} and LP_{02} modes. The diameters of the central low-index region, the upper boundary of the high-index region, the fiber core, and the cladding are 8.05, 12.45, 16.5,

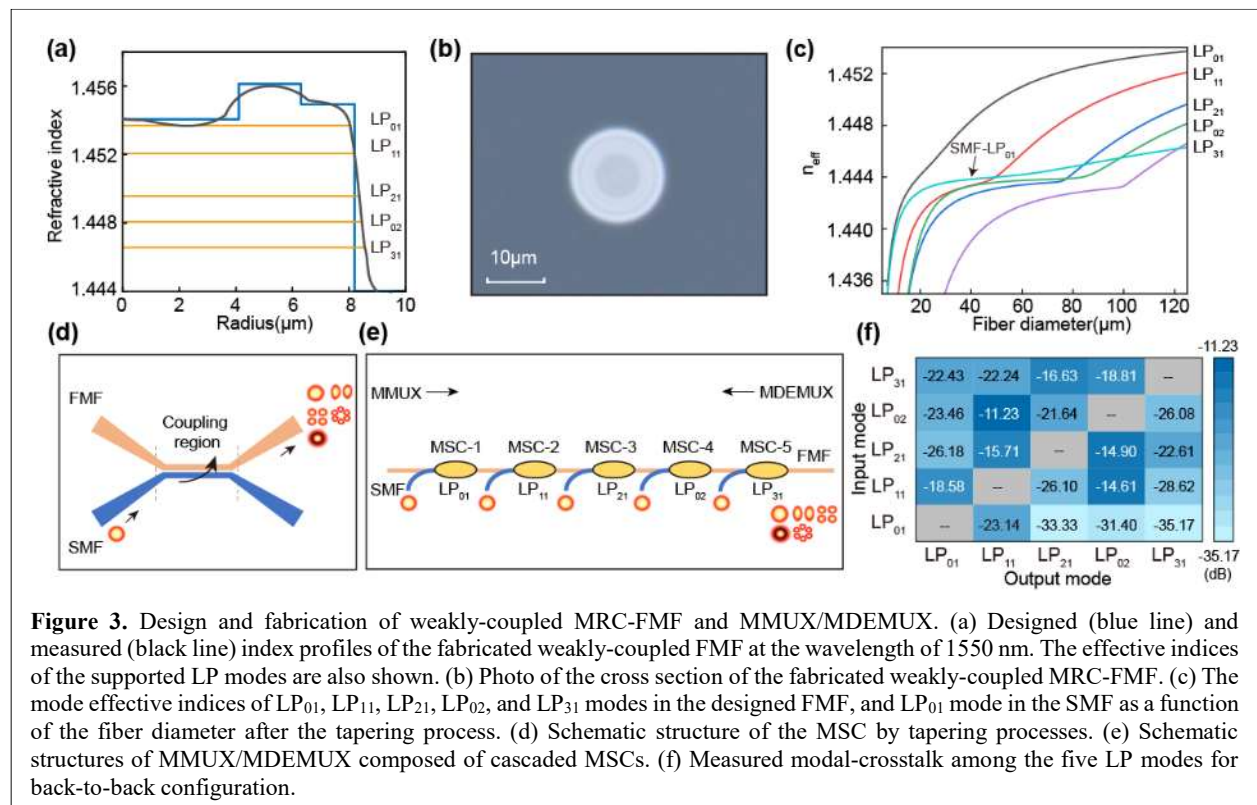


Figure 3. Design and fabrication of weakly-coupled MRC-FMF and MMUX/MDEMUX. (a) Designed (blue line) and measured (black line) index profiles of the fabricated weakly-coupled FMF at the wavelength of 1550 nm. The effective indices of the supported LP modes are also shown. (b) Photo of the cross section of the fabricated weakly-coupled MRC-FMF. (c) The mode effective indices of LP_{01} , LP_{11} , LP_{21} , LP_{02} , and LP_{31} modes in the designed FMF, and LP_{01} mode in the SMF as a function of the fiber diameter after the tapering process. (d) Schematic structure of the MSC by tapering processes. (e) Schematic structures of MMUX/MDEMUX composed of cascaded MSCs. (f) Measured modal-crosstalk among the five LP modes for back-to-back configuration.

and 125 μm , respectively. The relative index differences for the core of the initial step-index FMF, the low-index region, and the high-index region to the index of cladding are 0.748%, 0.688%, and 0.827%, respectively. The normalized frequency V is 5.95 and 6 LP modes are contained in the weakly-coupled MRC-FMF, among which the highest-order LP_{12} mode has large propagation loss and acts as a guarding mode. The photo of the cross section of the fabricated fiber is shown in Figure 3(b).

The matched MMUX and MDEMUX have the same structure composed of 5 cascaded MSCs but operate in opposite directions, as shown in Figure 3(e). Each MSC performs mode conversion between the fundamental mode of SMF and a specific LP mode in the MRC-FMF. The MSCs are fabricated by tapering parallel-placed MRC-FMF and SMF-28e fiber using a fused biconical taper platform (OSCOM, XQ-LZJ-B02) according to the phase-matching condition^[43], as shown in Figure 3(d). At the coupling region, light from the SMF could be coupled to a specific LP mode with high selectivity. Figure 3(c) illustrates the changes of n_{eff} for tapered SMF and MRC-FMF with different fiber diameters. The phase-matching conditions could be satisfied at the cross points in the curves, for which the corresponding values on the x-axis are the proper diameters for the tapered fibers. Different pre-tapering lengths for the MRC-FMF or the SMF should be applied to fabricate different MSCs. We can see that the n_{eff} of the LP_{01} mode in FMF is consistently higher than that of the LP_{01} mode in SMF. Therefore, pre-tapering the FMF is necessary for the LP_{01} MSC, while the SMF needs to be pre-tapered for the other MSCs.

The manufacturing of the MSCs involves two steps: pre-tapering the SMF or FMF to establish the initial diameter ratio of the two fibers, and then tapering the two fibers together maintaining the diameter ratio constant. The two fibers are heated using the hydroxide flame. Continuous-wave light at 1550 nm is injected into the SMF, and the power and mode field pattern

at the FMF output should be monitored during the second tapering process. The process is stopped when the output coupling power reaches its first maximum value. After the tapering process, the coupling region is pre-sealed and placed in a quartz groove, with the two ends fixed using thermosetting glue. Finally, a heat shrink tube is placed on the outer side of the quartz groove and heated to shrink it.

The modal-crosstalk matrix of the MMUX/MDEMUX in back-to-back configuration is also measured. In this configuration, the MMUX and MDEMUX are connected directly without passing any component. The mode crosstalk is measured by injecting 0-dBm optical power at 1550 nm into the input port of the MMUX and measuring the optical power at each output port of the MDEMUX. For a 5 LP mode MMUX/MDEMUX, the result is a 5×5 matrix with the diagonal elements being none and each of the remaining elements is calculated by the ratio of the measured output power of each LP mode to that of the target LP mode. The modal crosstalk for all five modes can be less than -11.23 dB as shown in Figure 3(f). The mode insertion losses of the MMUX/MDEMUX are also measured. For the insertion losses measurement of the MMUX, each time the probe light is injected into one single-mode input port of the cascaded five MSCs shown in Figure 3(e), the output power at the output FMF port is detected. For the insertion losses measurement of the MDEMUX, each time the MMUX is utilized to generate probe light for one of the five LP modes, the output power at the corresponding SMF output port is measured. For MMUX, the insertion losses of LP₀₁, LP₁₁, LP₂₁, LP₀₂, and LP₃₁ modes are 0.61, 2.48, 4.43, 4.84, and 7.01dB, respectively. For MDEMUX, the insertion losses of the five modes are 0.76, 2.61, 4.25, 4.42, and 7.21 dB, respectively.

Compared with the schematic diagram of the LP-mode synthesizer shown in Figure 1, we can see that the whole fiber ring laser could act as the LP-mode pool with selectable output light

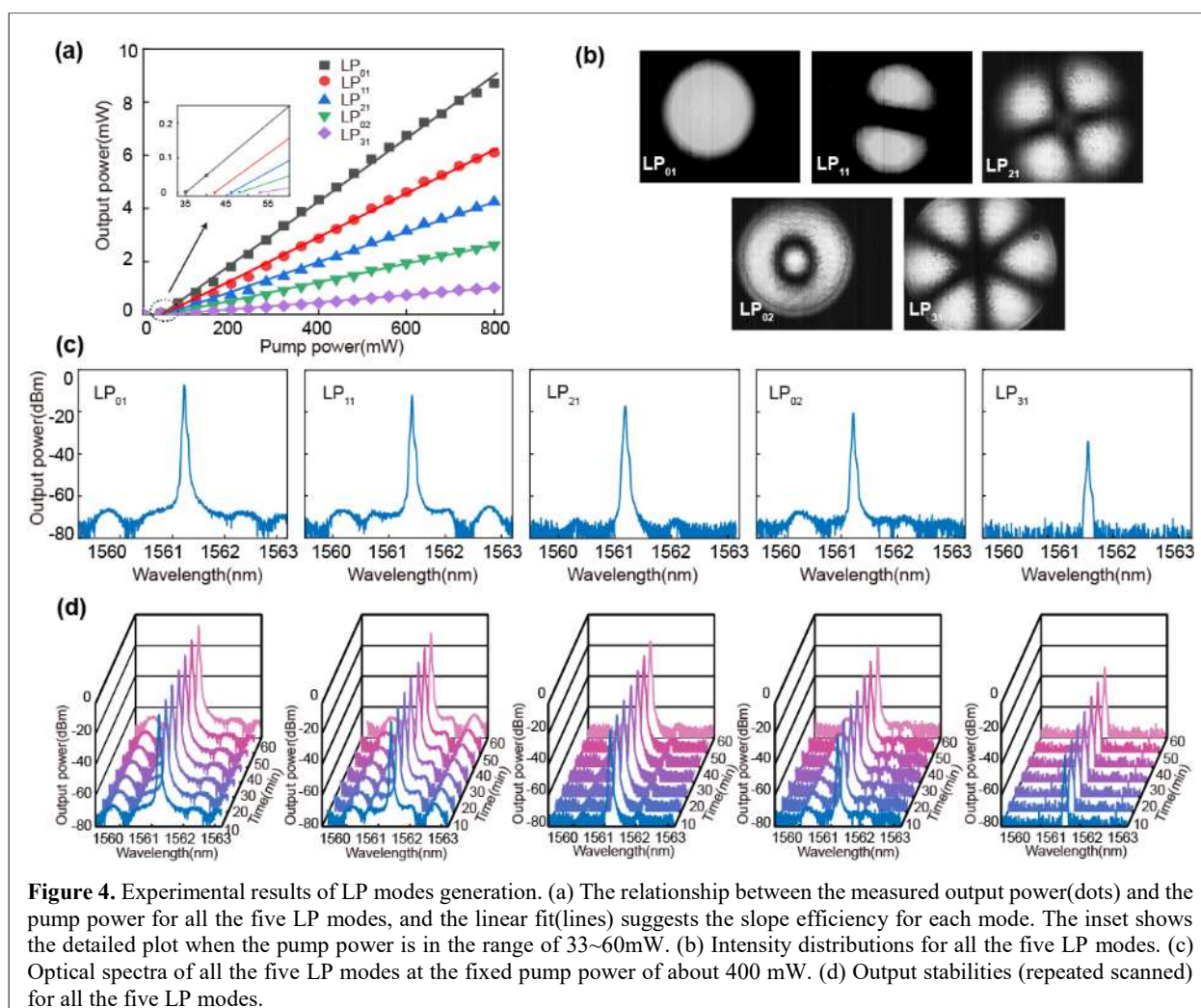
from one of the 5 LP modes, while the SM-OC-1 and the optical switching array (iseelink, GP-OSW1x16-SM-DT-FP) could bear the function of LP-mode selection unit. Because the output of the fiber ring laser is not polarization-maintained, we adopt a PC for polarization and phase control, which is realized by coiling a certain number of loops of MRC-FMF around a 3-paddle adjusting device. Each paddle could induce a fixed phase difference between polarization eigenmodes^[44]. For the operation to non-degenerate LP_{mn} ($m = 0$) modes (e.g., LP_{01} , LP_{02} modes), the PC is employed to modify the polarization components and apply phase difference between them by twisting the 3 paddles to reallocate and select electric fields. While for the case of operation to degenerate LP_{mn} ($m \geq 1$) modes (e.g., LP_{11} , LP_{21} , and LP_{31} modes), stress-induced birefringence in the PC can reallocate the optical power and apply phase difference among all 4-fold eigenmodes even if only even or odd mode is excited by the MMUX consisting of spatial-orientation-selective MSCs.^[44] Therefore, the PC provides the functions of both polarization and phase control and is manually controlled. The output of the 3-dB SM-OC-3 as a reference Gaussian beam is utilized to verify the generation of OAM lasing. The spectrum properties of the laser are measured by an optical spectrum analyzer (YOKOGAWA, AQ6370C) with a resolution of 0.02 nm. The output mode profiles are observed by a charge-coupled device (CCD) camera (Xenics, Bobcat-5316). The output power is measured by an optical power-meter (EXFO, FPM-302X-FOA-22).

IV. EXPERIMENTAL RESULTS

Experimental Results for LP Generation

The independent lasing for each LP mode of the proposed fiber ring laser is first investigated. The optical switching array is adjusted to excite each LP mode one by one, and the output power characteristics of output light at the 20% output port of the FM-OC are measured by the optical power-meter, while the intensity profile is measured by the CCD camera. The output signal power

224 versus the pump power for five lasing modes is plotted in Figure 4(a). We can see that the lasing
 225 output power for different LP modes increases linearly with the pump power when working above
 226 the lasing threshold. The slope efficiencies of 1.17%, 0.82%, 0.56%, 0.35%, and 0.13%, and the
 227 pump power thresholds of 35, 42, 46, 48, and 53 mW are obtained for LP₀₁, LP₁₁, LP₂₁, LP₀₂, and
 228 LP₃₁ lasing modes, respectively. The different values of slope efficiencies, and pump power
 229 thresholds among the five LP lasing modes are mainly influenced by different insertion losses for
 230 the five LP modes in the partial weakly-coupled FMF cavity. Higher slope efficiency can be
 231 achieved by reducing the insertion losses of the optical components especially those of the
 232 MMUX/MDEMUX. The intensity distributions of the LP modes are also recorded by the CCD



camera, and the results are shown in Figure 4(b).

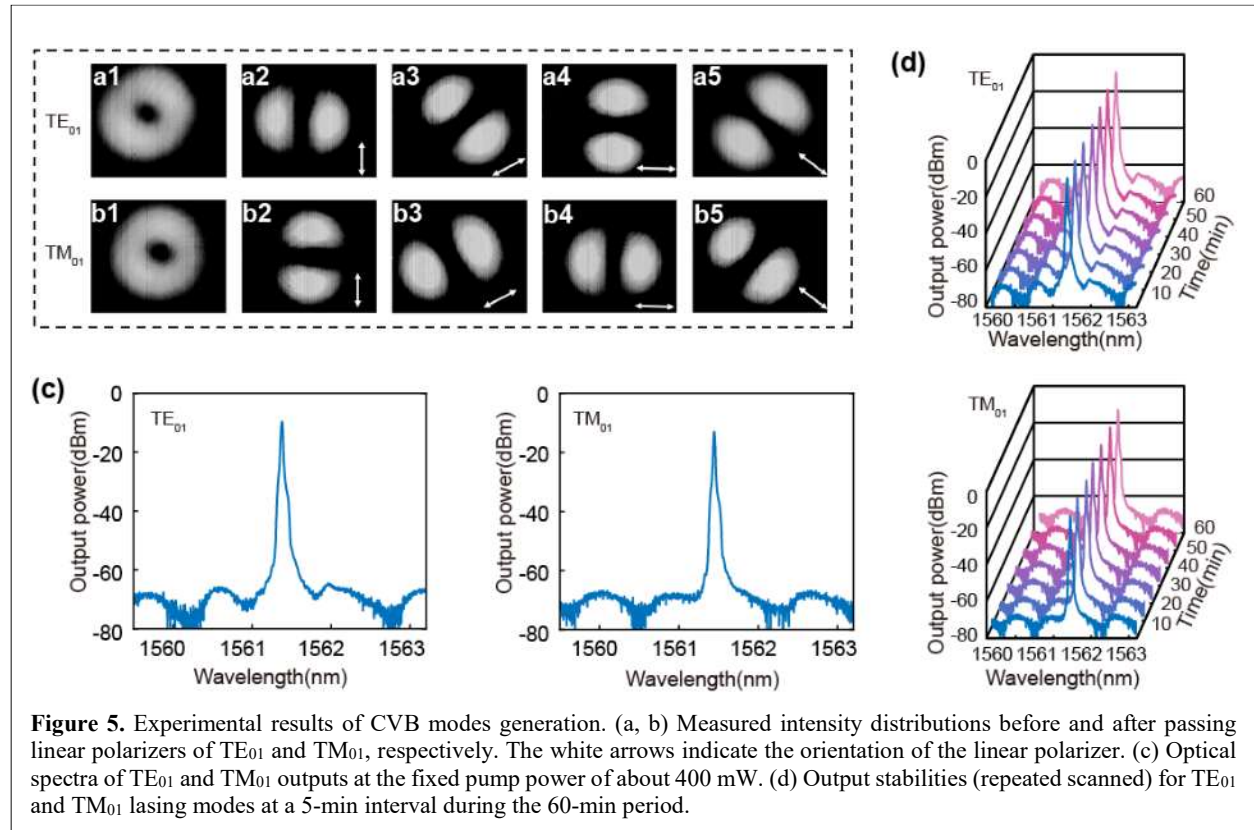
The spectral features and the stabilities of the lasing outputs are also investigated. Figure 4(c) shows the optical spectra of the lasing output of five LP modes measured by the optical spectrum analyzer when the pump power is fixed to be about 400 mW. The central wavelengths of 1561.23, 1561.41, 1561.18, 1561.25, and 1561.62 nm, the 3-dB linewidths of 0.028, 0.02, 0.028, 0.024, and 0.024 nm, the side-mode suppression ratios (SMSRs) of 59, 53, 53, 46, and 37 dB are achieved for the five LP modes from low to high orders, respectively. The wavelength differences come from the different effective lengths of lasing cavities for different LP modes. The residual spectra in LP_{01} and LP_{11} may arise from nonideal coupling of energy into adjacent modes at specific wavelengths during LP mode selection. The output stabilities for the five lasing LP modes are measured during the 60-min period at room temperature, and the output optical spectra are shown in Figure 4(d). The data are recorded at a 5-min interval over a 60-min period. The fluctuations of peak wavelength and average output power for each lasing LP mode are less than 0.032 nm and 0.055 mW, respectively.

Experimental Results for CVB Generation

Selectable generation of CVBs is demonstrated utilizing the proposed LP-mode synthesizer. According to the conversion relationship between LP modes and CVB modes by Equation (1), the LP_{11} mode is formed by the superposition of near-degenerate CVB modes including azimuthally-polarized TE_{01} , radially-polarized TM_{01} , and HE_{21}^e/HE_{21}^o modes. So, adjusting the optical switching array to only enable the lasing of LP_{11} modes, and then adjusting the PC to induce the rotation and extrusion, we could obtain the TE_{01} or TM_{01} mode. The intensity distributions of the output light are recorded by the CCD camera, and the results are shown in Figure 5(a) and Figure 5(b). The Figures 5(a1) and 5(b1) show the doughnut-shaped intensity profiles of both TE_{01} mode

and TM_{01} mode, respectively. In order to distinguish the polarization distributions of both CVB modes, a rotatable linear polarizer is placed in the light path between the lasing output and the CCD camera. Figures 5(a2) - (a5) & 5(b2) - (b5) show the intensity distributions with different polarization orientations (represented with white arrows) for the polarizer. The intensity patterns with two-lobe shape perpendicular to the orientation of the linear polarizer in Figures. 5(a2) - (a5) show that the output lasing beam is azimuthally-polarized TE_{01} mode, while the intensity patterns with two-lobe shape parallel to the orientation of the linear polarizer in Figures. 5(b2) - (b5) indicate that the light beam is radially-polarized TM_{01} mode.

Figure 5(c) presents the optical spectra of CVB outputs at the fixed pump power of about 400 mW. The central wavelengths of 1561.38 and 1561.45 nm, the 3-dB linewidths of 0.024 and 0.024 nm, and the SMSRs of 55 and 54 dB are measured for the TE_{01} and TM_{01} lasing modes, respectively. Figure 5(d) shows the output stabilities for TE_{01} and TM_{01} lasing modes at a 5-min



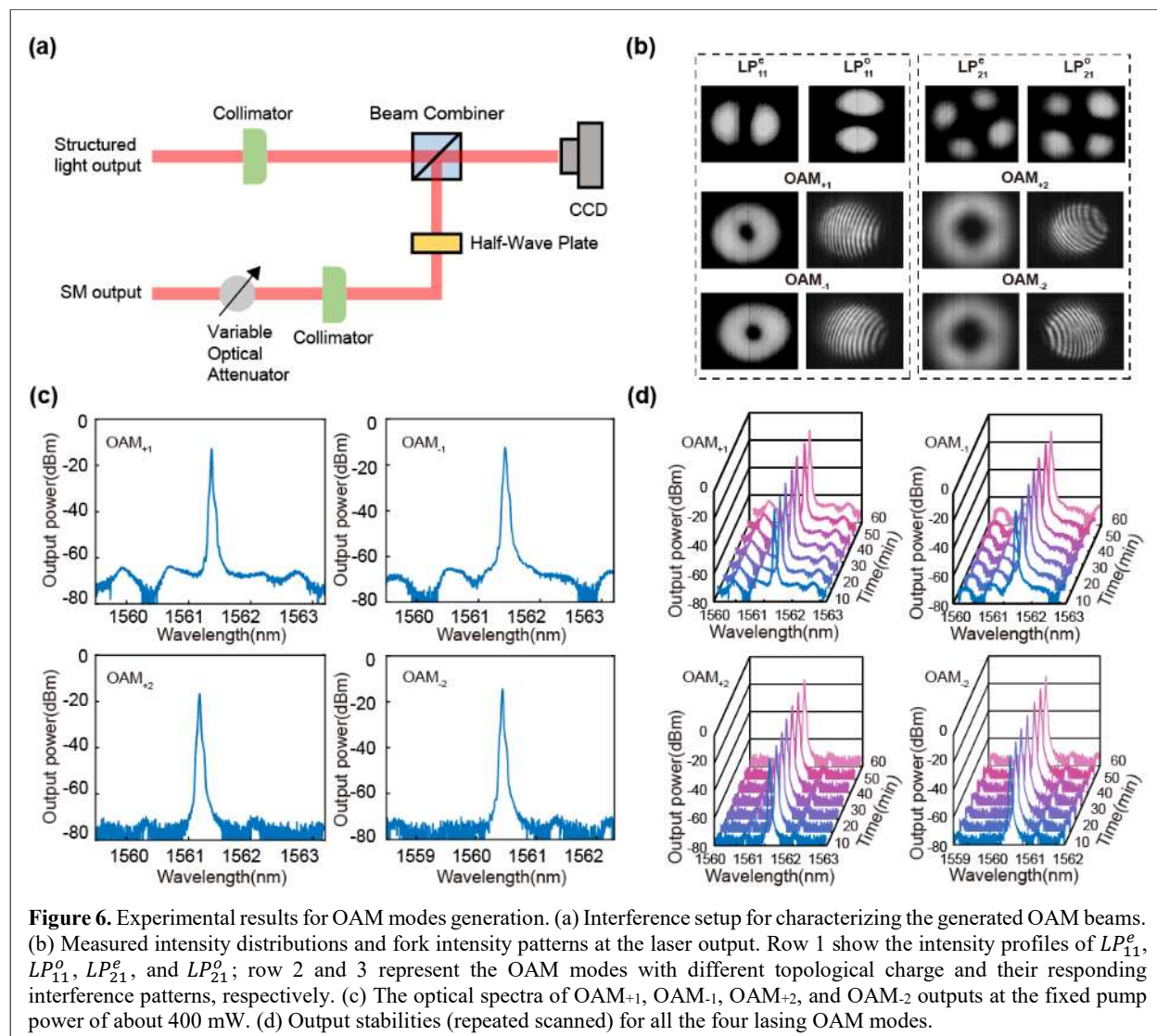
interval during the 60-min period. The peak wavelength fluctuation and the average output power fluctuation for TE₀₁ lasing mode are less than 0.044 nm and 0.042 mW, respectively. The fluctuations of peak wavelength and average output power for TM₀₁ lasing mode are less than 0.040 nm and 0.030 mW, respectively.

Experimental Results for OAM Generation

Selectable generation of OAMs is also verified utilizing the proposed LP-mode synthesizer. According to the conversion relationship by Equation (3), the linearly-polarized OAMs can be obtained by the superposition of a specific pair of degenerate LP modes in the weakly-guiding FMF under proper polarization and phase control. For example, $\vec{e}_x OAM_{\pm m} = \vec{e}_x LP_{m,1}^e \pm \vec{e}_x jLP_{m,1}^o$, it means that the x-polarized OAM modes can be obtained by combining the even and odd LP_{m,1} mode having the same polarized direction with a $\pm\pi/2$ phase shift. The $OAM_{\pm 1}$ could be obtained utilizing the $LP_{1,1}^e$ and $LP_{1,1}^o$, while the $OAM_{\pm 2}$ could be obtained utilizing the $LP_{2,1}^e$ and $LP_{2,1}^o$. So, the optical switching array should be adjusted to obtain the LP₁₁ or LP₂₁ lasing output for the generation of the $OAM_{\pm 1}$ or $OAM_{\pm 2}$, respectively. Then, the corresponding OAM beams will be obtained by tuning the PC's rotation angle and stress to induce the phase difference of $\pi/2$ between even and odd modes. Figure 6(a) shows the interference setup used to determine the topological charge number ($\pm 1, \pm 2$) of the generated OAM beams by observing their characteristic fork patterns with a CCD camera. The reference Gaussian beam at the output of SM-OC-3 is used for the interference setup to analyze the generated OAM beams. A free-space beam combiner combines both light to form the interference pattern and a variable optical attenuator balances the power of the two optical paths. A half-wave plate is used to adjust the polarization state of the reference Gaussian beam. By properly adjusting the PC, annular intensity profiles and their corresponding patterns could be observed. Figure 6(b) presents the measured intensity

distributions for LP modes and OAM beams, and fork intensity patterns at the laser output. The number of forks represents the topological charge of the OAM beams, which are $|m|=1,2$.

Figure 6(c) shows the optical spectra of the OAM_{+1} , OAM_{-1} , OAM_{+2} , and OAM_{-2} outputs at the fixed pump power of about 400 mW. The central wavelengths of 1561.39, 1561.43, 1561.18, and 1560.44 nm, the 3-dB linewidths of 0.020, 0.028, 0.032, and 0.028 nm, the SMSRs of 51, 53, 53, and 55 dB, are measured for the OAM_{+1} , OAM_{-1} , OAM_{+2} , and OAM_{-2} lasing modes, respectively. Figure 6(d) shows the output stabilities for all the four OAM lasing modes at a 5-min interval during the 60-min period. The fluctuations of peak wavelength for the OAM_{+1} , OAM_{-1} ,



OAM₊₂, and OAM₋₂ lasing modes are less than 0.048, 0.056, 0.072, and 0.060 nm, respectively, while the fluctuations of average output power are 0.072, 0.060, 0.041, and 0.058 mW, respectively.

V. CONCLUSION

In summary, we have proposed the concept of a programmable LP-mode synthesizer as a general way to generate CVB/OAM structured light according to their conversion relationship with LP modes. Based on a compact fiber ring laser generating switchable one of 5 LP modes and a PC for polarization and phase control, we successfully demonstrate the feasibility of the LP-mode synthesizer with the generation of TE₀₁, TM₀₁, OAM₊₁, OAM₋₁, OAM₊₂, and OAM₋₂ modes. Although the MMUX/MDEMUX will introduce additional insertion losses, it allows precise mode control of output light, which will greatly benefit high-power structure light applications. The programmable capability for the LP-mode synthesizer could be further realized by applying polarization-maintaining structures to the LP-mode pool. The mode purity of generated structure light could be monitored to improve the beam quality. The scheme may be further extended to other types of structured light such as Bessel beams. The proposed programmable synthesizer could take full advantage of mature LP mode manipulation schemes based on weakly-coupled FMFs and related optical components and is promising to be extended to wide applications.

Acknowledgment

This work was supported by the National Natural Science Foundation of China (U20A20160,62101009) and Peng Cheng Zili Project (PCL2023AS2-4).

Declaration of competing interest

The authors declare none.

References

1. B. J. Puttnam, G. Rademacher, and R. S. Luís, Space-division multiplexing for optical fiber communications, *Optica* **8**, 1186-1203 (2021).
2. G. B. Xavier and G. Lima, Quantum information processing with space-division multiplexing optical fibres, *Commun Phys* **3**, 9 (2020).
3. G. Milione, T. Wang, J. Han, and L. Bai, Remotely sensing an object's rotational orientation using the orbital angular momentum of light (Invited Paper), *Chin. Opt. Lett.* **15**, 030012-030016 (2017).
4. F. Pang, L. Xiang, H. Liu, L. Zhang, J. Wen, X. Zeng, and T. Wang, Review on Fiber-Optic Vortices and Their Sensing Applications, *J. Lightwave Technol.* **39**, 3740-3750 (2021).
5. B. M. Heffernan, P. S. Riley, O. D. Supekar, S. A. Meyer, D. Restrepo, M. E. Siemens, E. A. Gibson, and J. T. Gopinath, Two-photon, fiber-coupled, super-resolution microscope for biological imaging, *APL Photonics* **7**, 036102 (2022).
6. Z. H. Qian, J. M. Cui, X. W. Luo, Y. X. Zheng, Y. F. Huang, M. Z. Ai, R. He, C. F. Li, and G. C. Guo, Super-resolved Imaging of a Single Cold Atom on a Nanosecond Timescale, *Phys. Rev. Lett.* **127**, 263603 (2021).
7. Y. Li, L. M. Zhou, and N. Zhao, Anomalous motion of a particle levitated by Laguerre-Gaussian beams, *Opt. Lett.* **46**, 106-109 (2021).
8. M. Padgett, and R. Bowman, Tweezers with a twist, *Nature Photon* **5**, 343-348 (2011).
9. A. S. Ostrovsky, C. Rickenstroff-Parrao, and V. Arrizón, Generation of the 'perfect' optical vortex using a liquid-crystal spatial light modulator, *Opt. Lett.* **38**, 534-536 (2013).
10. Z. Y. Rong, Y. J. Han, S. Z. Wang, and C. S. Guo, Generation of arbitrary vector beams with cascaded liquid crystal spatial light modulators, *Opt. Express* **22**, 1636-1644 (2014).
11. L. Li, X. Zheng, C. Jin, M. Qi, X. Chen, Z. Ren, J. Bai, and Z. Sun, High repetition rate Q-switched radially polarized laser with a graphene-based output coupler, *Appl. Phys. Lett.* **105**, 221103 (2014).
12. Y. Xiang, S. Bai, and Z. Zhang, Cylindrical vector beam generation from a passively mode-locked Raman fiber laser, *Opt. Laser Technol.* **160**, 109079 (2023).

13. D. Naidoo, F. S. Roux, A. Dudley, I. Litvin, B. Piccirillo, L. Marrucci, and A. Forbes, Controlled generation of higher-order Poincaré sphere beams from a laser, *Nature Photon* **10**, 327-332 (2016).
14. G. Milione, H. I. Sztul, D. A. Nolan, J. Kim, M. Etienne, J. McCarthy, J. Wang, and R. R. Alfano, Cylindrical vector beam generation from a multi elliptical core optical fiber, in *CLEO:2011 - Laser Applications to Photonic Applications*, OSA Technical Digest (CD) (Optica Publishing Group, 2011), paper CTuB2.
15. M. W. Beijersbergen, R. P. Coerwinkel, M. Kristensen, and J. P. Woerdman, Helical-wavefront laser beams produced with a spiral phaseplate, *Opt. Commun.* **112**, 321-327 (1994).
16. S. Oemrawsingh, J. Houwelingen, E. Eliel, J. P. Woerdman, E. Versteegen, J. G. Kloosterboer, and G. Hooft, Production and characterization of spiral phase plates for optical wavelengths, *Appl. Opt.* **43**, 688-694(2004).
17. J. Feng, H. Shi, J. Yi, A. Zhang, S. Burokui, J. Chen, X. Chen, and Z. Xu, Generation of Tightly Focused Cylindrical Vector Beams with Dual-Channel Transmissive Metasurfaces, *Phys. Rev. Appl.* **19**, 044075 (2023).
18. E. Karimi, S. Schulz, I. Leon, H. Qassim, J. Upham, and R. Boyd, Generating optical orbital angular momentum at visible wavelengths using a plasmonic metasurface, *Light Sci. Appl.* **3**, e167 (2014).
19. H. Ahmed, H. Kim, Y. Zhang, Y. Intaravanne, J. Jang, J. Rho, S. Chen, and X. Chen, Optical metasurfaces for generating and manipulating optical vortex beams, *Nanophotonics* **11**, 941-956 (2022).
20. C. Li, T. Wieduwilt, F. J. Wendisch, A. Márquez, L. S. Menezes, S. A. Maier, M. A. Schmidt, and H. Ren, Metafiber transforming arbitrarily structured light, *Nat Commun* **14**, 7222 (2023).
21. W. Chang, M. Feng, B. Mao, P. Wang, Z. Wang, and Y. Liu, All-Fiber Fourth-Order OAM Mode Generation Employing a Long Period Fiber Grating Written By Preset Twist, *J. Lightwave Technol.* **40**, 4804-4811 (2022).
22. C. Jiang, K. Zhou, B. Sun, Y. Wan, Y. Ma, Z. Wang, Z. Zhang, C. Mou, and Y. Liu, Multiple core modes conversion using helical long-period fiber gratings, *Opt. Lett.* **48**, 2965-2968 (2023).

23. J. Lv, J. Lin, X. Ma, C. Dai, C. Gu, P. Yao, L. Xu, and Q. Zhan, Generation of cylindrical vector beams in a linear cavity mode-locked fiber laser based on nonlinear multimode interference, *Opt. Express*. **30**, 18320-18329 (2022).
24. Z. Xie, S. Gao, T. Lei., S. Feng, Y. Zhang, F. Li, J. Zhang, Z. Li, and X. Yuan, Integrated (de)multiplexer for orbital angular momentum fiber communication, *Photonics Res.* **6**, 743-749 (2018).
25. M. Zhang, J. Wen, Y. Wu, Y. Cao, Y. Luo, X. Zhang, F. Pang, W. Chen, and T. Wang, Generation and Amplification of Third-Order Orbital Angular Momentum Modes in a Low-Loss All-Fiber System, *IEEE Photonics J.* **15**, 1-7 (2023).
26. H. Wan, J. Wang, Z. Zhang, J. Wang, S. Ruan, and L. Zhang, Passively Mode-Locked Ytterbium-Doped Fiber Laser With Cylindrical Vector Beam Generation Based on Mode Selective Coupler, *J. Lightwave Technol.* **36**, 3403-3407 (2018).
27. D. Mao, Z. He, H. Lu, M. Li, W. Zhang, X. Cui, B. Jiang, and J. Zhao, All-fiber radially/azimuthally polarized lasers based on mode coupling of tapered fibers, *Opt. Lett.* **43**, 1590-1593 (2018).
28. D. Soma, S. Beppu, Y. Wakayama, K. Igarashi, T. Tsuritani, I. Morita, and M. Suzuki, 257-Tbit/s weakly coupled 10-mode C+ L-band WDM transmission, *J. Lightwave Technol.* **36**, 1375-1381, (2018).
29. D. Ge, Y. Gao, Y. Yang, L. Shen, Z. Li, Z. Chen, Y. He, and J. Li, A 6-LP-mode ultralow-modal-crosstalk double-ring-core FMF for weakly-coupled MDM transmission, *Opt. Commun.* **451**, 97-103 (2019).
30. M. Zuo, D. Ge, J. Liu, Y. Gao, L. Shen, X. Lan, Z. Chen, Y. He, and J. Li, Long-haul intermodal-MIMO-free MDM transmission based on a weakly coupled multiple-ring-core few-mode fiber, *Opt. Express*. **30**, 5868-5878 (2022).
31. B. Huang, N. K. Fontaine, R. Ryf, B. Guan, S. G. Leon-Saval, R. Shubochkin, Y. Sun, R. Lingle, and G. Li, All-fiber mode-group selective photonic lantern using graded-index multimode fibers, *Opt. Express* **23**, 224-234 (2015).
32. S. G. Leon-Saval, N. K. Fontaine, J. R. Salazar-Gil, B. Ercan, R. Ryf, and J. Bland-Hawthorn, Mode-selective photonic lanterns for space-division multiplexing, *Opt. Express*. **22**, 1036-1044 (2014).

33. G. Labroille, B. Denolle, P. Jian, P. Genevieux, N. Treps, and J. Morizur, Efficient and mode selective spatial mode multiplexer based on multi-plane light conversion, *Opt. Express*. **22**, 15599-15607 (2014).
34. G. Labroille, P. Jian, N. Barré, B. Denolle, and J. Morizur, Mode Selective 10-Mode Multiplexer based on Multi-Plane Light Conversion, in *Optical Fiber Communication Conference, OSA Technical Digest (online) (Optica Publishing Group, 2016)*, paper Th3E.5.
35. K. Aoki, A. Okamoto, Y. Wakayama, A. Tomita, and S. Honma, Selective multimode excitation using volume holographic mode multiplexer, *Opt. Lett.* **5**, 769-771 (2013).
36. J. Cui, Y. Gao, S. Huang, J. Yu, J. Liu, J. Jia, Y. He, Z. Chen, and J. Li, Five-LP-Mode IM/DD MDM Transmission Based on Degenerate-Mode-Selective Couplers With Side-Polishing Processing, *J. Lightwave Technol.* **41**, 2991-2998 (2023).
37. Y. Gao, J. Cui, D. Ge, J. Jia, C. Du, C. Xia, Y. Liu, Z. Li, Y. He, Z. Chen, J. Li, and G. Li, A degenerate-mode-selective coupler for stable DSP-free MDM transmission, *J. Lightwave Technol.* **37**, 4410-4420 (2019).
38. Q. Zhan, Cylindrical vector beams: from mathematical concepts to applications, *Adv. Opt. Photonics* **1**, 1-57 (2009).
39. L. Allen, M. W. Beijersbergen, R. Spreeuw, and J. P. Woerdman, Orbital angular momentum of light and the transformation of Laguerre-Gaussian laser modes, *Phys. Rev. A* **45**, 8185-8189 (1992).
40. S. Ramachandran and P. Kristensen, Optical vortices in fiber, *Nanophotonics* **2**, 455-474 (2013).
41. Y. Han, Y.G. Liu, W. Huang, Z. Wang, J. Guo, and M. Luo, Generation of linearly polarized orbital angular momentum modes in a side-hole ring fiber with tunable topology numbers, *Opt. Express* **24**, 17272-17284 (2016).
42. F. Ren, X. Huang and J. Wang, Fused-fiber-based 3-dB mode insensitive power splitters for few-mode optical fiber networks, *Opt. Eng* **56**(11), 116101 (2017).
43. R. Ismaeel, T. Lee, B. Oduro, Y. Jung, and G. Brambilla, All-fiber fused directional coupler for highly efficient spatial mode conversion, *Opt. Express* **22**, 11610 (2014).
44. H. C. Lefèvre, Single-mode fiber fractional wave devices and polarization controllers, *Electron. Lett* **16**, 778-780 (1980).